EUROPEAN ORGANIZATION FOR NUCLEAR RESEARCH

CERN-EP/98-52
2 April 1998

Search for the Standard Model Higgs Boson in e^+e^- Interactions at $\sqrt{s} = 183$ GeV

L3 Collaboration

Abstract

A search for the Standard Model Higgs boson is performed with the L3 detector at LEP. The data sample, corresponding to a luminosity of 55.3 pb^{-1}, was collected at an average centre-of-mass energy of 182.7 GeV. No Higgs signal is observed, leading to a lower limit on the Higgs boson mass of 87.6 GeV at the 95% confidence level.

Submitted to *Phys.Lett. B*

1 Introduction

The mechanism of spontaneous symmetry breaking [1] in the Standard Model [2] gives rise to a fundamental neutral scalar particle, the Higgs boson. In the Standard Model the mass of the Higgs boson, M_{H}, is not predicted. Higgs searches in the mass range up to 70 GeV have been reported by L3 [3] and by other experiments [4]. In this paper, we present the results of a Higgs search using a data sample collected at an average centre-of-mass energy of 182.7 GeV that extends the sensitivity to significantly larger Higgs boson masses.

At present LEP energies, the main production mechanism is the Higgs-strahlung process:

$$\mathrm{e^+e^-} \rightarrow \mathrm{Z}^* \rightarrow \mathrm{HZ}\,. \tag{1}$$

In addition to process (1), there is a small contribution from the $\mathrm{W^+W^-}$ and ZZ fusion reactions to the $\mathrm{H}\nu\bar{\nu}$ and $\mathrm{He^+e^-}$ final states, respectively. The main background sources are $\mathrm{e^+e^-} \rightarrow \mathrm{q\bar{q}}(\gamma)$ and four-fermion final states from $\mathrm{e^+e^-} \rightarrow \mathrm{W^+W^-}$ and $\mathrm{e^+e^-} \rightarrow \mathrm{ZZ}$.

2 Data and Monte Carlo Samples

The data were collected by the L3 detector [5] at LEP in 1997. The integrated luminosity is 55.3 pb^{-1} at an average centre-of-mass energy $\sqrt{s} = 182.7$ GeV.

The signal cross section is calculated using the HZHA generator [6]. For the efficiency studies samples of Higgs events are generated using PYTHIA [7] for Higgs masses between 65 and 93 GeV, with a mass step of at most 2 GeV. Between 2000 and 5000 events per final state are generated at each Higgs mass. For the background studies the following Monte Carlo programs are used: PYTHIA ($\mathrm{e^+e^-} \rightarrow \mathrm{q\bar{q}}(\gamma)$, $\mathrm{e^+e^-} \rightarrow \mathrm{ZZ}$), KORALW [8] ($\mathrm{e^+e^-} \rightarrow \mathrm{W^+W^-}$), KORALZ [9] ($\mathrm{e^+e^-} \rightarrow \tau^+\tau^-$), PYTHIA and PHOJET [10] ($\mathrm{e^+e^-} \rightarrow \mathrm{e^+e^-q\bar{q}}$), and EXCALIBUR [11] ($\mathrm{e^+e^-} \rightarrow \mathrm{f\,\bar{f}'f\,\bar{f}'}$). The number of simulated background events for the most important background channels corresponds to at least 100 times the collected luminosity.

The L3 detector response is simulated using the GEANT 3.15 program [12], which takes into account the effects of energy loss, multiple scattering and showering in the detector. The GHEISHA program [13] is used to simulate hadronic interactions in the detector.

3 Analysis Procedures

The search for the Standard Model Higgs boson at LEP involves four distinct event topologies produced in the process $\mathrm{e^+e^-} \rightarrow \mathrm{HZ}$, namely $\mathrm{q\bar{q}q\bar{q}}$, $\mathrm{q\bar{q}}\nu\bar{\nu}$, $\mathrm{q\bar{q}}\ell^+\ell^-$ ($\ell = \mathrm{e}, \mu, \tau$) and $\tau^+\tau^-\mathrm{q\bar{q}}$. Each topology requires its own optimised selection criteria. Since it is expected that a large fraction (~84%) of Higgs decays contain b-hadrons, the selection criteria for hadronic Higgs decays are optimised for the $\mathrm{H} \rightarrow \mathrm{b\bar{b}}$ final states.

At least two independent analyses are carried out for each event topology. The analyses are optimised using approximately one half of the signal and background Monte Carlo samples. The analysis performances are then evaluated using the other half of the Monte Carlo samples. All the analyses show similar performance and are described in detail in reference [14]. We briefly describe here the neural network analysis, used for all channels, except for the $\mathrm{HZ} \rightarrow \mathrm{q\bar{q}}\tau^+\tau^-$ and $\mathrm{HZ} \rightarrow \tau^+\tau^-\mathrm{q\bar{q}}$ channels, for which a cut-based analysis is used. In both analyses a preselection is chosen to reduce background while keeping the signal efficiency high. All analyses subject the events satisfying the selection criteria to a kinematic fit that imposes energy-momentum conservation. The constraint that one of the two reconstructed invariant masses in the event be close to M_{Z} is also applied. For Higgs masses between 80 and 90 GeV the mass resolution ranges from 1.5 to 3 GeV [14] depending on the final state.

In the neural network analyses event variables are combined into a feed forward neural network [15], with a number of inputs, hidden nodes and outputs which depends on the specific channel being investigated. All channels include an event b-tagging variable and the χ^2 of the event kinematic fit, χ^2_{fit}. The event b-tagging variable is a combination of jet b-tagging probabilities for all the jets in the event [3].

The shape of the neural network output is made independent of the Higgs mass hypothesis. This is achieved as follows: all the measured variables which depend on the Higgs mass are divided by the corresponding quantities resulting from the kinematic fit. The reconstructed Higgs mass, $M^{\mathrm{H}}_{\mathrm{rec}}$, as calculated from the kinematic fit, is combined with the output of the neural network, NN_{out}, into the purity variable P_M for a given Higgs mass hypothesis M_{H}. The purity is defined as follows:

$$P_M = \frac{N_{\mathrm{s}} \cdot f_{\mathrm{s}}(M^{\mathrm{H}}_{\mathrm{rec}}, M_{\mathrm{H}}) \cdot g_{\mathrm{s}}(NN_{\mathrm{out}})}{N_{\mathrm{s}} \cdot f_{\mathrm{s}}(M^{\mathrm{H}}_{\mathrm{rec}}, M_{\mathrm{H}}) \cdot g_{\mathrm{s}}(NN_{\mathrm{out}}) + N_{\mathrm{b}} \cdot f_{\mathrm{b}}(M^{\mathrm{H}}_{\mathrm{rec}}, M_{\mathrm{H}}) \cdot g_{\mathrm{b}}(NN_{\mathrm{out}})} \ . \qquad (2)$$

In Eq. (2) N_{s} and N_{b} are the number of expected signal and background events after preselection, f_{s} and g_{s} are the one-variable probability density functions of $M^{\mathrm{H}}_{\mathrm{rec}}$ and NN_{out} for the signal, respectively. The corresponding functions for the background are denoted by f_{b} and g_{b}.

In the cut-based analysis of $\mathrm{q\bar{q}}\tau^+\tau^-$ and $\tau^+\tau^-\mathrm{q\bar{q}}$, a tighter set of preselection cuts is used. The variables with the largest distinguishing power between signal and background are the two b-tagging variables of the jets and the χ^2 of the mass, $\chi^2_{M_{\mathrm{H}}} = (M^{\mathrm{H}}_{\mathrm{rec}} - M_{\mathrm{H}})^2/\sigma^2_{M^{\mathrm{H}}_{\mathrm{rec}}}$. They are used to define three probabilities F_{J_1}, F_{J_2} and F_M [14]. The final discriminant variable is defined as

$$\begin{aligned} D_M &= \log\left(F_M \cdot F_{J_1} \cdot F_{J_2}\right), && \text{for HZ} \rightarrow \mathrm{q\bar{q}}\tau^+\tau^- \text{ selection;} \\ D_M &= \log\left(F_M\right), && \text{for HZ} \rightarrow \tau^+\tau^-\mathrm{q\bar{q}} \text{ selection.} \end{aligned} \qquad (3)$$

4 Event Selection

4.1 The HZ $\rightarrow \mathrm{q\bar{q}}\,\mathrm{q\bar{q}}$ channel

The signature of these events is four high multiplicity jets. Two of these jets usually contain b quarks and the other two have an invariant mass consistent with the Z mass.

First, high multiplicity hadronic events with at least 10 tracks and at least 30 calorimetric clusters are selected, with the visible energy $110 < E_{\mathrm{vis}} < 250$ GeV and missing momentum $P_{\mathrm{mis}} < 45$ GeV. If the maximum energy of a lepton or a photon in the event exceeds 60 GeV, the event is rejected.

Jets are reconstructed using the JADE clustering scheme [16] with the parameter $Y_{\mathrm{cut}} = 0.02$. Events containing at least four jets are selected. They are then forced to four jets using the DURHAM [17] algorithm. A kinematic fit imposing four-momentum conservation is applied to the four jets to improve the di-jet mass resolution. Then a mass χ^2 is defined as

$$\chi^2_{M_{\mathrm{H}}} = \frac{(\Sigma_M - M_{\mathrm{Z}} - M_{\mathrm{H}})^2}{\sigma^2_{\Sigma}} + \frac{(\delta_M - |M_{\mathrm{Z}} - M_{\mathrm{H}}|)^2}{\sigma^2_{\delta}} \ . \qquad (4)$$

The variables Σ_M and δ_M are the sum and the difference of the di-jet masses for each of the three possible combinations. Their resolutions are $\sigma_\Sigma = 3$ GeV and $\sigma_\delta = 5$ GeV. The di-jet combination which gives the minimum $\chi^2_{M_{\mathrm{H}}}$ is chosen and the pair of jets with the mass closest to M_{Z} is assigned to the Z. The opening angle between the Z jets is required to exceed 103°.

A total of 321 events pass the preselection, while 315 are expected from the background processes, with 22% of the events from $\mathrm{q\bar{q}}(\gamma)$ process, 75% from WW production, and the rest from ZZ production. The selection efficiency is estimated to be 65% for an 87 GeV Higgs signal. Selection efficiencies for other Higgs mass values are given in Table 1. The discriminant variable NN_{out} is constructed using a neural network with 12 input nodes, 24 hidden nodes and 1 output node. The inputs include multiplicity of tracks and clusters, event shape variables, b-tagging variables and the event χ^2_{fit}. The event B_{tag} distribution for the selected events is shown in Figure 1a. The neural network output spectrum is presented in Figure 1b. Its shape is almost independent of the Higgs mass. The invariant mass distribution for events with $NN_{\mathrm{out}} > 0.5$ is presented in Figure 1c. No indication for a Higgs signal is observed in the mass range under investigation. The purity distribution for the selected events is shown in Figure 1d. One of the most significant candidates is shown in Figure 2.

4.2 The HZ $\rightarrow \mathrm{q\bar{q}}\nu\bar{\nu}$ channel

The signature of this process is two acoplanar hadronic jets, usually containing b-quarks, no isolated leptons and large missing transverse momentum.

High multiplicity hadronic events with at least 4 charged tracks and at least 15 calorimetric clusters are selected. The energy in the forward calorimeters is required to be smaller than 15 GeV. All clusters in the event are combined to form two hadronic jets using the DURHAM algorithm [17]. The invariant mass of these jets is required to be between 40 and 115 GeV and each jet must be at least 16° away from the beam axis. These cuts reduce contributions from pure leptonic final states and from two-photon interactions, $\mathrm{e^+e^-} \rightarrow \mathrm{e^+e^-q\bar{q}}$, while keeping a significant fraction of hadronic events from $\mathrm{e^+e^-} \rightarrow \mathrm{q\bar{q}}(\gamma)$, $\mathrm{W^+W^-}$ and ZZ production.

To further reject events from the fermion pair production process $\mathrm{e^+e^-} \rightarrow \mathrm{q\bar{q}}(\gamma)$, the transverse momentum is required to exceed 5 GeV. The missing momentum vector must be at least 16° away from the beam axis and the longitudinal momentum must be smaller than 70% of the visible energy. The opening angle between the two jets is required to be greater than 69°. The recoiling invariant mass must be between 50 and 130 GeV. The event B_{tag} variable (Figure 3a) is required to exceed 0.6.

A total of 56 events are selected in data with 50.4 expected background and 74% signal efficiency for an 87 GeV Higgs (see Table 1 for other Higgs masses). The discriminant variable is constructed using a neural network with 8 input nodes, 15 hidden nodes and 1 output node. The inputs include B_{tag}, angular information, recoiling mass, the two jet masses, transverse imbalance and the event χ^2_{fit}. The neural network output distribution, the invariant mass distribution for events with $NN_{\mathrm{out}} > 0.5$ and the distribution of the purity variable P_M are shown in Figures 3b, 3c and 3d, respectively. No indication for a Higgs signal is observed.

4.3 The HZ $\rightarrow \mathrm{q\bar{q}}\ell^+\ell^-$ ($\ell = \mathrm{e}, \mu$) channels

The signature of $\mathrm{HZ} \rightarrow \mathrm{q\bar{q}e^+e^-}$ and $\mathrm{HZ} \rightarrow \mathrm{q\bar{q}}\mu^+\mu^-$ production is an event with a pair of high energy electrons or muons, with an invariant mass close to M_{Z}, accompanied by two hadronic jets.

High multiplicity hadronic events are selected with at least 4 tracks and 20 calorimetric clusters. A pair of isolated electrons or muons must be present. The energy of each lepton is required to exceed 15 GeV. The invariant mass of the lepton pair is required to be between 40 and 110 GeV for electrons and between 35 and 125 GeV for muons. If there are more than two lepton candidates, the two with the highest energies are considered. The opening angle between the two leptons is required to exceed 103° for electrons and 86° for muons. The invariant mass of hadronic jets is required to be between 35 and 125 GeV and the opening angle between the jets must exceed 86°.

In the $\mathrm{q\bar{q}e^+e^-}$ channel, 6 events are observed in the data while 5.4 events are expected from background, with an efficiency of 75% for an 87 GeV Higgs signal. In the $\mathrm{q\bar{q}}\mu^+\mu^-$ channel, 2 events are observed in the data while 1.4 events are expected from background, with an efficiency of 45% for an 87 GeV Higgs signal (see Table 1 for more details). The discriminant variable is constructed using a neural network with 6 input nodes, 10 hidden nodes, and 1 output node. The inputs include the event B_{tag}, angular information, invariant mass of leptons and jets and the event χ^2_{fit}. The combined neural network output spectrum for electrons and muons is presented in Figure 4a. The invariant mass distribution for events with $NN_{\mathrm{out}} > 0.1$ is presented in Figure 4b. Only one $\mathrm{HZ} \rightarrow \mathrm{q\bar{q}\,e^+e^-}$ candidate event satisfies this requirement. No indication for a Higgs signal is observed. The neural network output and the invariant mass are combined in the purity variable P_M, as defined in Eq.2.

4.4 The $\mathrm{HZ} \rightarrow \tau^+\tau^-\,\mathrm{q\bar{q}}$ and $\mathrm{HZ} \rightarrow \mathrm{q\bar{q}}\,\tau^+\tau^-$ channels

The signatures of $\mathrm{HZ} \rightarrow \tau^+\tau^-\mathrm{q\bar{q}}$ and $\mathrm{HZ} \rightarrow \mathrm{q\bar{q}}\,\tau^+\tau^-$ events are similar to those of the $\mathrm{HZ} \rightarrow \mathrm{q\bar{q}}\ell^+\ell^-$ ($\ell = \mathrm{e}, \mu$) channels.

Tau leptons are identified as low multiplicity jets comprising 1 or 3 tracks and not more than 5 calorimetric clusters in a cone of 10° half-opening angle around the jet direction. The measured energy of the decay particles should be at least 4 GeV. The charges of tau candidates are required to be one and opposite.

As isolation criteria, no more than 3 tracks are allowed in a cone of 30° half-opening angle around the tau-jet direction and the ratio of the energy measured in the range from 10° to 30° to the energy measured in the range from 0° to 10° around the direction of the tau-jet should not exceed 0.3.

High multiplicity hadronic events are selected with at least 9 tracks and 15 calorimetric clusters. Two jets and two tau candidates with a separation angle of at least 10° are required. The effective centre-of-mass energy [3] should be within $0.5 \leq \sqrt{s'}/\sqrt{s} \leq 0.97$ and the missing momentum vector must be larger than 5 GeV.

The invariant mass of the jets, M_{jj}, is computed. The invariant mass of the two tau candidates, $M_{\tau\tau}$, is computed as the recoil mass to the jets. Then, using the distribution of the jet b-tag variables and of the $\chi^2_{M_\mathrm{H}}$ calculated with $M^{\mathrm{H}}_{\mathrm{rec}} = M_{\mathrm{jj}}$ and $M^{\mathrm{H}}_{\mathrm{rec}} = M_{\tau\tau}$, the probabilities for both hypotheses are computed and the most likely combination is retained. The reconstructed Z mass is required to be between 60 and 118 GeV. A kinematic fit is performed imposing four momentum conservation and the Z mass constraint for $M_{\tau\tau}$ or M_{jj}, depending on the event classification. Events with a χ^2_{fit} larger than 20 are rejected. Finally, the discriminant variable D_M is computed using $\chi^2_{M_\mathrm{H}}$ and jet b-tagging distributions, as described in Section 3.

Signal efficiencies for different Higgs masses, background expectations and the number of observed data events are compared in Table 1. For each of the two final states with $\tau^+\tau^-$, two numbers are given for each Higgs mass value. The first is the signal efficiency of the selection designed for that specific final state. The second, in parenthesis, is the cross efficiency of the selection designed for the other final state. The distributions of the mass probability F_M and of the reconstructed Higgs mass $M^{\mathrm{H}}_{\mathrm{rec}}$, for the combined $\mathrm{q\bar{q}}\tau^+\tau^-$ and $\tau^+\tau^-\mathrm{q\bar{q}}$ final states, are shown in Figures 4c and 4d, respectively.

5 Errors on signal and background predictions

The error on the predicted numbers of signal and background events arises from three different sources: uncertainties on the production cross sections, on the detector response and limited Monte Carlo statistics.

Theoretical errors on the Higgs boson production cross section due to the uncertainties in M_{top} and α_s [18] ($\sim 0.1\%$), interference effects [19] ($\sim 1\%$) and errors on Higgs decay branching fractions due to quark masses [20] ($\sim 1\%$) introduce an uncertainty on the predicted number of signal events. Experimental uncertainties in the LEP centre-of-mass energy of ± 0.029 GeV [21] and in the luminosity measurements of 0.3% account for an additional 0.3% systematic error on the number of expected signal events.

The main sources of systematic error due to uncertainties in the detector response include uncertainties on the energy scale of the individual subdetectors, on the global energy scale, on the tracking efficiency and on the b-tagging efficiency. Their magnitude is evaluated by comparing control data samples with the Monte Carlo predictions. The uncertainties on the energy scales are estimated using the samples of radiative return to the Z and WW events. The systematic uncertainty due to the b-tagging is assigned using the calibration sample of hadronic events at 91 GeV and assuming that the difference between data and Monte Carlo distributions is entirely due to the systematic effects. An overall systematic error on the number of signal events of 4% is evaluated assuming that all the above uncertainties are independent.

The systematic error on the expected number of background events is due to the uncertainty on both the cross sections and the selection efficiency for the background processes. The overall systematic error on the predicted background is estimated to be 10% . It is assumed to be fully correlated between the different search channels.

The statistical error on the predicted number of both signal and background events due to limited Monte Carlo statistics is taken into account in the limit calculation.

6 Results

No statistically significant excess of Higgs-like events is observed by any of the analyses. For illustration purposes, the reconstructed Higgs mass distribution of the 11 most significant candidates is shown in Figure 5, where the corresponding distributions for an 87 GeV Higgs signal and for the background are also shown for comparison. A total of 10.6 events are expected from background processes.

The distributions of the purity P_M for the channels $\mathrm{HZ} \to \mathrm{q\bar{q}q\bar{q}}$, $\mathrm{q\bar{q}}\nu\bar{\nu}$, $\mathrm{q\bar{q}e^+e^-}$ and $\mathrm{q\bar{q}}\mu^+\mu^-$ and the distributions of the discriminant variable D_M, for the $\mathrm{HZ} \to \mathrm{q\bar{q}}\tau^+\tau^-$ and $\mathrm{HZ} \to \tau^+\tau^-\,\mathrm{q\bar{q}}$ channels are used in the likelihood function from which the confidence level is derived using the technique described in reference [3]. Only bins with a signal-over-background ratio greater than 0.1 are used in the final confidence level calculation [14].

The confidence level (CL) is calculated using a large number of Monte Carlo experiments. The systematic errors on the signal and background expectations are taken into account during the generation of these Monte Carlo experiments. In each trial experiment, the total number of signal and background events is smeared according to a Gaussian distribution with standard deviation equal to their respective total statistical and systematic error.

The measured (1-CL) as a function of the Higgs boson mass is shown in Figure 6a. The 1-CL values are calculated for Higgs mass hypotheses separated by 0.1 GeV using statistically independent Monte Carlo samples. To reduce statistical fluctuations at each point, an interpolation between a few neighbouring points is applied. Also shown is the median of the (1-CL) distribution derived from a sample of Monte Carlo experiments, simulated according to the background spectra only. The (1-CL) distribution is asymmetric; however the probability that, in absence of a signal, the actual CL will be higher than the median is 50%, by definition. The median represents the sensitivity of the search and reaches 95% CL at 86.8 GeV. For comparison the average confidence level line reaches 95% CL at 85.0 GeV. For Figure 6, the data taken at the Z resonance, at $\sqrt{s} = 161 - 172$ GeV [3] and the data at $\sqrt{s} = 183$ GeV, presented in this paper, are combined.

The number of expected signal events and number of signal events excluded at 95% confidence level as a function of the Higgs boson mass are presented in Figure 6b. The lower limit on the Higgs boson mass is

$$M_{\mathrm{H}} > 87.6 \text{ GeV} \quad \text{at} \quad 95\% \text{ CL}.$$

The probability to obtain a higher limit is estimated to be 35%. The new lower limit on the Higgs boson mass improves and supersedes our previously published results [3].

Acknowledgements

We wish to express our gratitude to the CERN accelerator divisions for the excellent performance of the LEP machine. We acknowledge the efforts of all engineers and technicians who have participated in the construction and maintenance of this experiment.

References

[1] P.W.Higgs, Phys.Lett. **12** (1964) 132;
F.Englert and R.Brout, Phys.Rev.Lett. **13** (1964) 321;
G.S.Guralnik *et al.*, Phys.Rev.Lett. **13** (1964) 585.

[2] S.L.Glashow, Nucl.Phys. **22** (1961) 579;
S.Weinberg, Phys.Rev.Lett. **19** (1967) 1264;
A.Salam, "Elementary Particle Theory", Ed. N. Svartholm, Stockholm, "Almquist and Wiksell", (1968), 367.

[3] M. Acciarri *et al.*, L3 Collaboration, Phys.Lett. **B411** (1997) 373.

[4] R.Barate *et al.*, ALEPH Collaboration, Phys.Lett. **B412** (1997) 155;
P.Abreu *et al.*, DELPHI Collaboration, Eur.Phys.Journ. **C2** (1998) 1;
K.Ackerstaff *et al.*, OPAL Collaboration, Eur.Phys.Journ. **C1** (1998) 425.

[5] L3 Collaboration, B.Adeva *et al.*, Nucl.Instr.Meth. **A289** (1990) 35;
J.A.Bakken *et al.*, Nucl.Instr.Meth. **A275** (1989) 81;
O.Adriani *et al.*, Nucl.Instr.Meth. **A302** (1991) 53;
B.Adeva *et al.*, Nucl.Instr.Meth. **A323** (1992) 109;
K.Deiters *et al.*, Nucl.Instr.Meth. **A323** (1992) 162;
M.Chemarin *et al.*, Nucl.Instr.Meth. **A349** (1994) 345;
B.Acciari *et al.*, Nucl.Instr.Meth. **A351** (1994) 300;
G.Basti *et al.*, Nucl.Instr.Meth. **A374** (1996) 293;
A.Adam *et al.*, Nucl.Instr.Meth. **A383** (1996) 342.

[6] P.Janot, "The HZHA generator", in "Physics at LEP2", Eds. G.Altarelli, T.Sjöstrand and F.Zwirner, CERN 96-01 (1996) Vol.2, 309.

[7] T.Sjöstrand, CERN-TH/7112/93 (1993), revised August 1995;
T.Sjöstrand, Comp.Phys.Comm. **82** (1994) 74.

[8] M.Skrzypek *et al.*, Comp.Phys.Comm. **94** (1996) 216;
M.Skrzypek *et al.*, Phys.Lett. **B372** (1996) 289.

[9] S.Jadach, B.F.L.Ward and Z.Wąs, Comp.Phys.Comm. **79** (1994) 503.

[10] R.Engel, Z.Phys. **C66** (1995) 203;
R.Engel, J.Ranft and S.Roesler, Phys.Rev. **D52** (1995) 1459.

[11] F.A.Berends, R.Pittau and R.Kleiss, Comp.Phys.Comm. **85** (1995) 437.

[12] R.Brun *et al.*, preprint CERN DD/EE/84-1 (Revised 1987).

[13] H.Fesefeldt, RWTH Aachen Report PITHA 85/02 (1985).

[14] M.Biasini *et al.*, "Standard Model Higgs searches at $\sqrt{s} = 183$ GeV, L3 Note 2241, March 24, 1998 [1)].

[1)] This L3 Note is freely available on request from: The L3 secretariat, CERN, CH–1211 Geneva 23, Switzerland. Internet: http://l3www.cern.ch/l3pubanddoc.html

[15] L.Lönnblad, C. Peterson and T.Rognvaldsson, Nucl.Phys. **B349** (1991) 675; C.Peterson *et al.*, Comp.Phys.Comm. **81** (1994) 185.

[16] S.Catani *et al.*, Phys.Lett. **B263** (1991) 491.

[17] S.Bethke *et al.*, Nucl.Phys. **B370** (1992) 310.

[18] B.A.Kniehl, Phys.Rep. **240 C** (1994) 211; E.Gross, B.A.Kniehl and G.Wolf, Z.Phys. **C63** (1994) 417; *erratum-ibid* **C66** (1995) 321.

[19] M.Krämer, W.Kilian and P.M.Zerwas, Phys.Lett. **B373** (1996) 135.

[20] A.Djouadi *et al.*, Z.Phys. **C70** (1996) 427.

[21] The Working Group on LEP Energy, "Preliminary LEP energy calibration for 1997 data", LEP Energy Group Note 98-01.

The L3 Collaboration:

M.Acciarri[28] O.Adriani[17] M.Aguilar-Benitez[27] S.Ahlen[12] J.Alcaraz[27] G.Alemanni[23] J.Allaby[18] A.Aloisio[30] M.G.Alviggi[30] G.Ambrosi[20] H.Anderhub[49] V.P.Andreev[7,38] T.Angelescu[14] F.Anselmo[10] A.Arefiev[29] T.Azemoon[3] T.Aziz[11] P.Bagnaia[37] L.Baksay[44] S.Banerjee[11] Sw.Banerjee[11] K.Banicz[46] A.Barczyk[49,47] R.Barillère[18] L.Barone[37] P.Bartalini[23] A.Baschirotto[28] M.Basile[10] R.Battiston[34] A.Bay[23] F.Becattini[17] U.Becker[16] F.Behner[49] J.Berdugo[27] P.Berges[16] B.Bertucci[34] B.L.Betev[49] S.Bhattacharya[11] M.Biasini[34] A.Biland[49] G.M.Bilei[34] J.J.Blaising[4] S.C.Blyth[35] G.J.Bobbink[2] R.Bock[1] A.Böhm[1] L.Boldizsar[15] B.Borgia[18,37] D.Bourilkov[49] M.Bourquin[20] S.Braccini[20] J.G.Branson[40] V.Brigljevic[49] I.C.Brock[35] A.Buffini[17] A.Buijs[45] J.D.Burger[16] W.J.Burger[34] J.Busenitz[44] A.Button[3] X.D.Cai[16] M.Campanelli[49] M.Capell[16] G.Cara Romeo[10] G.Carlino[30] A.M.Cartacci[17] J.Casaus[27] G.Castellini[17] F.Cavallari[37] N.Cavallo[30] C.Cecchi[20] M.Cerrada[27] F.Cesaroni[24] M.Chamizo[27] Y.H.Chang[51] U.K.Chaturvedi[19] S.V.Chekanov[32] M.Chemarin[26] A.Chen[51] G.Chen[8] G.M.Chen[8] H.F.Chen[21] H.S.Chen[8] X.Chereau[4] G.Chiefari[30] C.Y.Chien[5] L.Cifarelli[39] F.Cindolo[10] C.Civinini[17] I.Clare[16] R.Clare[16] G.Coignet[4] A.P.Colijn[2] N.Colino[27] S.Costantini[9] F.Cotorobai[14] B.de la Cruz[27] A.Csilling[15] T.S.Dai[16] R.D'Alessandro[17] R.de Asmundis[30] A.Degré[4] K.Deiters[47] D.della Volpe[30] P.Denes[36] F.DeNotaristefani[37] M.Diemoz[37] D.van Dierendonck[2] F.Di Lodovico[49] C.Dionisi[18,37] M.Dittmar[49] A.Dominguez[40] A.Doria[30] M.T.Dova[19,♯] D.Duchesneau[4] P.Duinker[2] I.Duran[41] S.Easo[34] H.El Mamouni[26] A.Engler[35] F.J.Eppling[16] F.C.Erné[2] J.P.Ernenwein[26] P.Extermann[20] M.Fabre[47] R.Faccini[37] M.A.Falagan[27] S.Falciano[37] A.Favara[17] J.Fay[26] O.Fedin[38] M.Felcini[49] T.Ferguson[35] F.Ferroni[37] H.Fesefeldt[1] E.Fiandrini[34] J.H.Field[20] F.Filthaut[18] P.H.Fisher[16] I.Fisk[40] G.Forconi[16] L.Fredj[20] K.Freudenreich[49] C.Furetta[28] Yu.Galaktionov[29,16] S.N.Ganguli[11] P.Garcia-Abia[6] M.Gataullin[33] S.S.Gau[13] S.Gentile[37] N.Gheordanescu[14] S.Giagu[37] S.Goldfarb[23] J.Goldstein[12] Z.F.Gong[21] A.Gougas[5] G.Gratta[33] M.W.Gruenewald[9] R.van Gulik[2] V.K.Gupta[36] A.Gurtu[11] L.J.Gutay[46] D.Haas[6] B.Hartmann[1] A.Hasan[31] D.Hatzifotiadou[10] T.Hebbeker[9] A.Hervé[18] P.Hidas[15] J.Hirschfelder[35] W.C.van Hoek[32] H.Hofer[49] H.Hoorani[35] S.R.Hou[51] G.Hu[5] I.Iashvili[48] B.N.Jin[8] L.W.Jones[3] P.de Jong[18] I.Josa-Mutuberria[27] R.A.Khan[19] D.Kamrad[48] J.S.Kapustinsky[25] Y.Karyotakis[4] M.Kaur[19,♢] M.N.Kienzle-Focacci[20] D.Kim[37] D.H.Kim[43] J.K.Kim[43] S.C.Kim[43] W.W.Kinnison[25] A.Kirkby[33] D.Kirkby[33] J.Kirkby[18] D.Kiss[15] W.Kittel[32] A.Klimentov[16,29] A.C.König[32] A.Kopp[48] I.Korolko[29] V.Koutsenko[16,29] R.W.Kraemer[35] W.Krenz[1] A.Kunin[16,29] P.Lacentre[48,♮,♯] P.Ladron de Guevara[27] I.Laktineh[26] G.Landi[17] C.Lapoint[16] K.Lassila-Perini[49] P.Laurikainen[22] A.Lavorato[39] M.Lebeau[18] A.Lebedev[16] P.Lebrun[26] P.Lecomte[49] P.Lecoq[18] P.Le Coultre[49] H.J.Lee[9] J.M.Le Goff[18] R.Leiste[48] E.Leonardi[37] P.Levtchenko[38] C.Li[21] C.H.Lin[51] W.T.Lin[51] F.L.Linde[2,18] L.Lista[30] Z.A.Liu[8] W.Lohmann[48] E.Longo[37] W.Lu[33] Y.S.Lu[8] K.Lübelsmeyer[1] C.Luci[18,37] D.Luckey[16] L.Luminari[37] W.Lustermann[49] W.G.Ma[21] M.Maity[11] G.Majumder[11] L.Malgeri[18] A.Malinin[29] C.Maña[27] D.Mangeol[32] P.Marchesini[49] G.Marian[44,§] A.Marin[12] J.P.Martin[26] F.Marzano[37] G.G.G.Massaro[2] K.Mazumdar[11] R.R.McNeil[7] S.Mele[18] L.Merola[30] M.Meschini[17] W.J.Metzger[32] M.von der Mey[1] D.Migani[10] A.Mihul[14] A.J.W.van Mil[32] H.Milcent[18] G.Mirabelli[37] J.Mnich[18] P.Molnar[9] B.Monteleoni[17] R.Moore[3] T.Moulik[11] R.Mount[33] F.Muheim[20] A.J.M.Muijs[2] S.Nahn[16] M.Napolitano[30] F.Nessi-Tedaldi[49] H.Newman[33] T.Niessen[1] A.Nippe[23] A.Nisati[37] H.Nowak[48] Y.D.Oh[43] G.Organtini[37] R.Ostonen[22] S.Palit[13] C.Palomares[27] D.Pandoulas[1] S.Paoletti[37] P.Paolucci[30] H.K.Park[35] I.H.Park[43] G.Pascale[37] G.Passaleva[18] S.Patricelli[30] T.Paul[13] M.Pauluzzi[34] C.Paus[18] F.Pauss[49] D.Peach[18] Y.J.Pei[1] S.Pensotti[28] D.Perret-Gallix[4] B.Petersen[32] S.Petrak[9] A.Pevsner[5] D.Piccolo[30] M.Pieri[17] P.A.Piroué[36] E.Pistolesi[28] V.Plyaskin[29] M.Pohl[49] V.Pojidaev[29,17] H.Postema[16] J.Pothier[18] N.Produit[20] D.Prokofiev[38] J.Quartieri[39] G.Rahal-Callot[49] N.Raja[11] P.G.Rancoita[28] M.Rattaggi[28] G.Raven[40] P.Razis[31] D.Ren[49] M.Rescigno[37] S.Reucroft[13] T.van Rhee[45] S.Riemann[48] K.Riles[3] A.Robohm[49] J.Rodin[44] B.P.Roe[3] L.Romero[27] S.Rosier-Lees[4] S.Roth[1] J.A.Rubio[18] D.Ruschmeier[9] H.Rykaczewski[49] J.Salicio[18] E.Sanchez[27] M.P.Sanders[32] M.E.Sarakinos[22] C.Schäfer[1] V.Schegelsky[38] S.Schmidt-Kaerst[1] D.Schmitz[1] N.Scholz[49] H.Schopper[50] D.J.Schotanus[32] J.Schwenke[1] G.Schwering[1] C.Sciacca[30] D.Sciarrino[20] L.Servoli[34] S.Shevchenko[33] N.Shivarov[42] V.Shoutko[29] J.Shukla[25] E.Shumilov[29] A.Shvorob[33] T.Siedenburg[1] D.Son[43] B.Smith[16] P.Spillantini[17] M.Steuer[16] D.P.Stickland[36] A.Stone[7] H.Stone[36] B.Stoyanov[42] A.Straessner[1] K.Sudhakar[11] G.Sultanov[19] L.Z.Sun[21] G.F.Susinno[20] H.Suter[49] J.D.Swain[19] X.W.Tang[8] L.Tauscher[6] L.Taylor[13] Samuel C.C.Ting[16] S.M.Ting[16] S.C.Tonwar[11] J.Tóth[15] C.Tully[36] K.L.Tung[8] Y.Uchida[16] J.Ulbricht[49] E.Valente[37] G.Vesztergombi[15] I.Vetlitsky[29] G.Viertel[49] M.Vivargent[4] S.Vlachos[6] H.Vogel[35] H.Vogt[48] I.Vorobiev[18,29] A.A.Vorobyov[38] A.Vorvolakos[31] M.Wadhwa[6] W.Wallraff[1] J.C.Wang[16] X.L.Wang[21] Z.M.Wang[21] A.Weber[1] S.X.Wu[16] S.Wynhoff[1] J.Xu[12] Z.Z.Xu[21] B.Z.Yang[21] C.G.Yang[8] H.J.Yang[8] M.Yang[8] J.B.Ye[21] S.C.Yeh[52] J.M.You[35] An.Zalite[38] Yu.Zalite[38] P.Zemp[49] Y.Zeng[1] Z.P.Zhang[21] B.Zhou[12] G.Y.Zhu[8] R.Y.Zhu[33] A.Zichichi[10,18,19] F.Ziegler[48] G.Zilizi[44,§]

1 I. Physikalisches Institut, RWTH, D-52056 Aachen, FRG[§]
III. Physikalisches Institut, RWTH, D-52056 Aachen, FRG[§]
2 National Institute for High Energy Physics, NIKHEF, and University of Amsterdam, NL-1009 DB Amsterdam, The Netherlands
3 University of Michigan, Ann Arbor, MI 48109, USA
4 Laboratoire d'Annecy-le-Vieux de Physique des Particules, LAPP,IN2P3-CNRS, BP 110, F-74941 Annecy-le-Vieux CEDEX, France
5 Johns Hopkins University, Baltimore, MD 21218, USA
6 Institute of Physics, University of Basel, CH-4056 Basel, Switzerland
7 Louisiana State University, Baton Rouge, LA 70803, USA
8 Institute of High Energy Physics, IHEP, 100039 Beijing, China[△]
9 Humboldt University, D-10099 Berlin, FRG[§]
10 University of Bologna and INFN-Sezione di Bologna, I-40126 Bologna, Italy
11 Tata Institute of Fundamental Research, Bombay 400 005, India
12 Boston University, Boston, MA 02215, USA
13 Northeastern University, Boston, MA 02115, USA
14 Institute of Atomic Physics and University of Bucharest, R-76900 Bucharest, Romania
15 Central Research Institute for Physics of the Hungarian Academy of Sciences, H-1525 Budapest 114, Hungary[‡]
16 Massachusetts Institute of Technology, Cambridge, MA 02139, USA
17 INFN Sezione di Firenze and University of Florence, I-50125 Florence, Italy
18 European Laboratory for Particle Physics, CERN, CH-1211 Geneva 23, Switzerland
19 World Laboratory, FBLJA Project, CH-1211 Geneva 23, Switzerland
20 University of Geneva, CH-1211 Geneva 4, Switzerland
21 Chinese University of Science and Technology, USTC, Hefei, Anhui 230 029, China[△]
22 SEFT, Research Institute for High Energy Physics, P.O. Box 9, SF-00014 Helsinki, Finland
23 University of Lausanne, CH-1015 Lausanne, Switzerland
24 INFN-Sezione di Lecce and Universitá Degli Studi di Lecce, I-73100 Lecce, Italy
25 Los Alamos National Laboratory, Los Alamos, NM 87544, USA
26 Institut de Physique Nucléaire de Lyon, IN2P3-CNRS,Université Claude Bernard, F-69622 Villeurbanne, France
27 Centro de Investigaciones Energeticas, Medioambientales y Tecnologicas, CIEMAT, E-28040 Madrid, Spain♭
28 INFN-Sezione di Milano, I-20133 Milan, Italy
29 Institute of Theoretical and Experimental Physics, ITEP, Moscow, Russia
30 INFN-Sezione di Napoli and University of Naples, I-80125 Naples, Italy
31 Department of Natural Sciences, University of Cyprus, Nicosia, Cyprus
32 University of Nijmegen and NIKHEF, NL-6525 ED Nijmegen, The Netherlands
33 California Institute of Technology, Pasadena, CA 91125, USA
34 INFN-Sezione di Perugia and Universitá Degli Studi di Perugia, I-06100 Perugia, Italy
35 Carnegie Mellon University, Pittsburgh, PA 15213, USA
36 Princeton University, Princeton, NJ 08544, USA
37 INFN-Sezione di Roma and University of Rome, "La Sapienza", I-00185 Rome, Italy
38 Nuclear Physics Institute, St. Petersburg, Russia
39 University and INFN, Salerno, I-84100 Salerno, Italy
40 University of California, San Diego, CA 92093, USA
41 Dept. de Fisica de Particulas Elementales, Univ. de Santiago, E-15706 Santiago de Compostela, Spain
42 Bulgarian Academy of Sciences, Central Lab. of Mechatronics and Instrumentation, BU-1113 Sofia, Bulgaria
43 Center for High Energy Physics, Adv. Inst. of Sciences and Technology, 305-701 Taejon, Republic of Korea
44 University of Alabama, Tuscaloosa, AL 35486, USA
45 Utrecht University and NIKHEF, NL-3584 CB Utrecht, The Netherlands
46 Purdue University, West Lafayette, IN 47907, USA
47 Paul Scherrer Institut, PSI, CH-5232 Villigen, Switzerland
48 DESY-Institut für Hochenergiephysik, D-15738 Zeuthen, FRG
49 Eidgenössische Technische Hochschule, ETH Zürich, CH-8093 Zürich, Switzerland
50 University of Hamburg, D-22761 Hamburg, FRG
51 National Central University, Chung-Li, Taiwan, China
52 Department of Physics, National Tsing Hua University, Taiwan, China
§ Supported by the German Bundesministerium für Bildung, Wissenschaft, Forschung und Technologie
‡ Supported by the Hungarian OTKA fund under contract numbers T019181, F023259 and T024011.
§ Also supported by the Hungarian OTKA fund under contract numbers T22238 and T026178.
♭ Supported also by the Comisión Interministerial de Ciencia y Technologı́a.
♯ Also supported by CONICET and Universidad Nacional de La Plata, CC 67, 1900 La Plata, Argentina.
♮ Supported by Deutscher Akademischer Austauschdienst.
◇ Also supported by Panjab University, Chandigarh-160014, India.
△ Supported by the National Natural Science Foundation of China.

Table 1: The signal efficiencies for various Higgs masses, the background expectations and the number of data events. In parentheses the cross-efficiencies for the two tau channels are given.

Final state		Efficiency for M_{H} =					BG	DATA
H	Z	75 GeV	80 GeV	85 GeV	87 GeV	90 GeV		
$\mathrm{q\bar{q}}$	$\mathrm{q\bar{q}}$	0.61	0.65	0.66	0.65	0.66	315	321
$\mathrm{q\bar{q}}$	$\nu\bar{\nu}$	0.76	0.76	0.75	0.74	0.71	50.4	56
$\mathrm{q\bar{q}}$	$\mathrm{e^+e^-}$	0.77	0.78	0.80	0.75	0.77	5.4	6
$\mathrm{q\bar{q}}$	$\mu^+\mu^-$	0.41	0.44	0.45	0.45	0.48	1.4	2
$\mathrm{q\bar{q}}$	$\tau^+\tau^-$	0.17(0.06)	0.15(0.06)	0.14(0.08)	0.15(0.08)	0.14(0.08)	0.7	0
$\tau^+\tau^-$	$\mathrm{q\bar{q}}$	0.20(0.03)	0.19(0.06)	0.17(0.07)	0.16(0.09)	0.16(0.09)	1.7	1

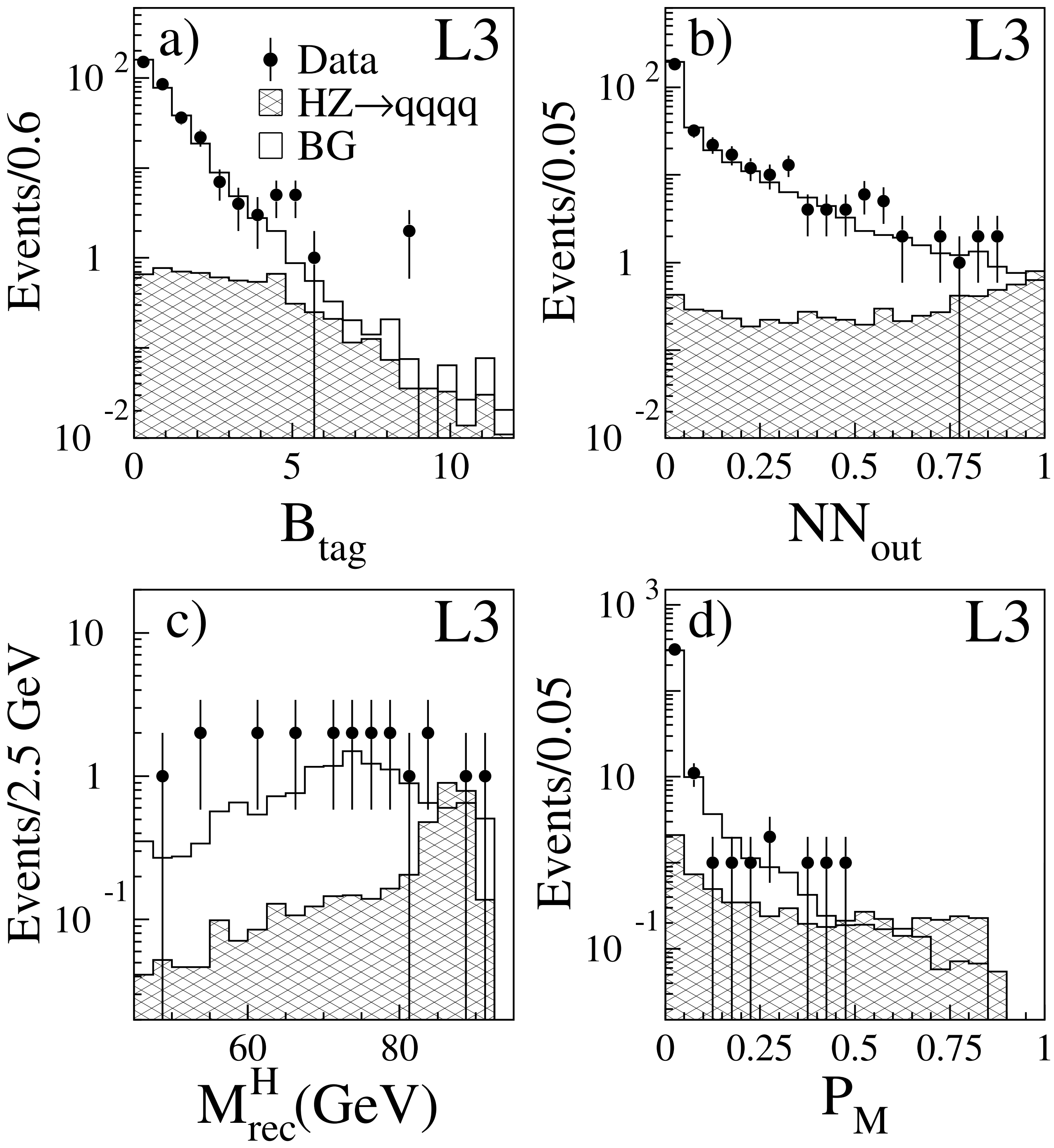

Figure 1: Distributions, shown after the preselection for the $q\bar{q}\,q\bar{q}$ channel, of (a) the event $B_{\rm tag}$, (b) the neural network output $NN_{\rm out}$, (c) the invariant mass (for events with $NN_{\rm out} > 0.5$) and (d) the purity. The dots indicate the data, the empty histograms show the background expectations, while the superimposed hatched histograms correspond to a 87 GeV Higgs signal normalised to the Standard Model cross section.

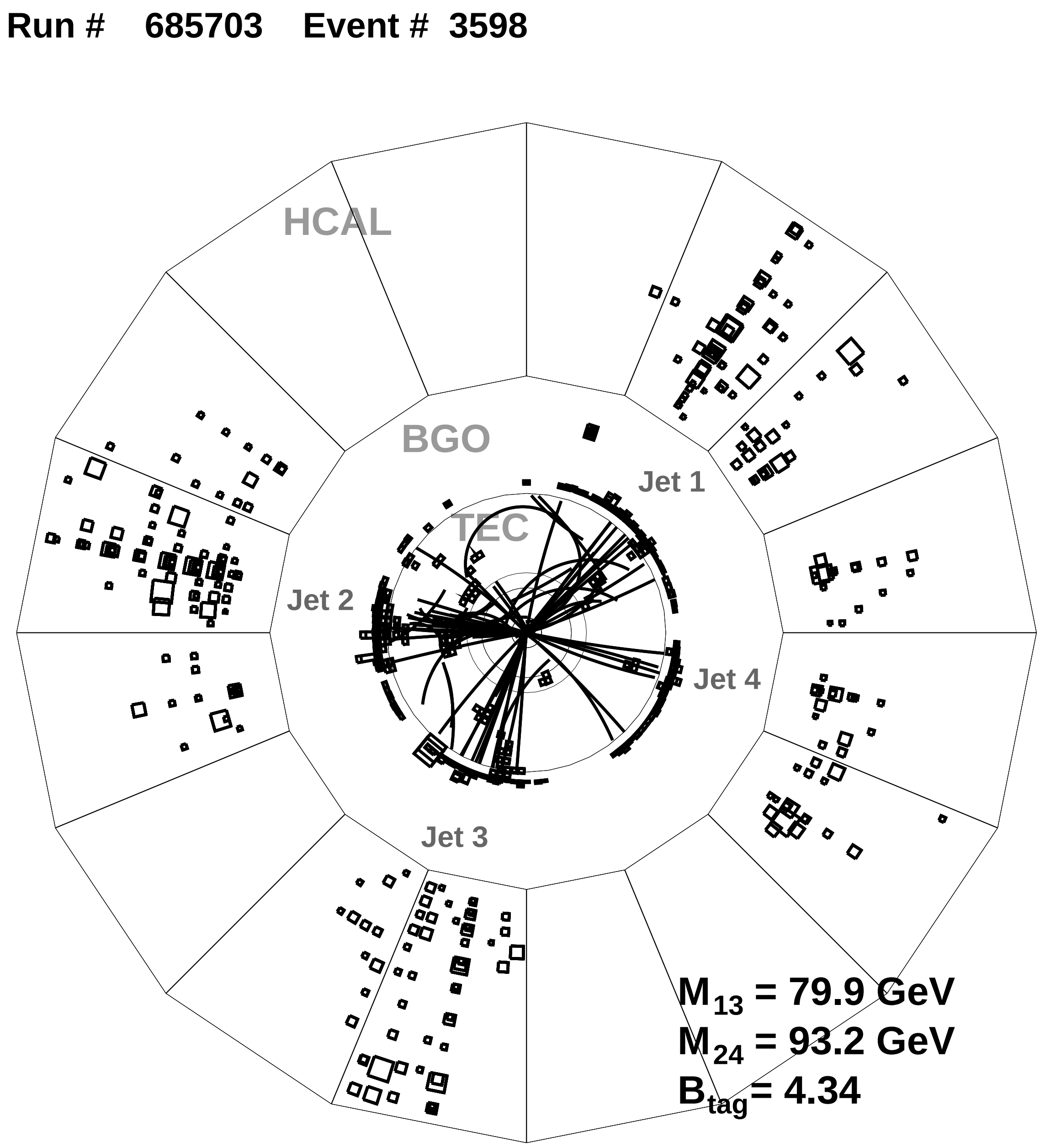

Figure 2: A candidate $q\bar{q}\,q\bar{q}$ event. The invariant masses of jet pairs are reconstructed to be 79.9 GeV and 93.2 GeV for H and Z jets respectively.

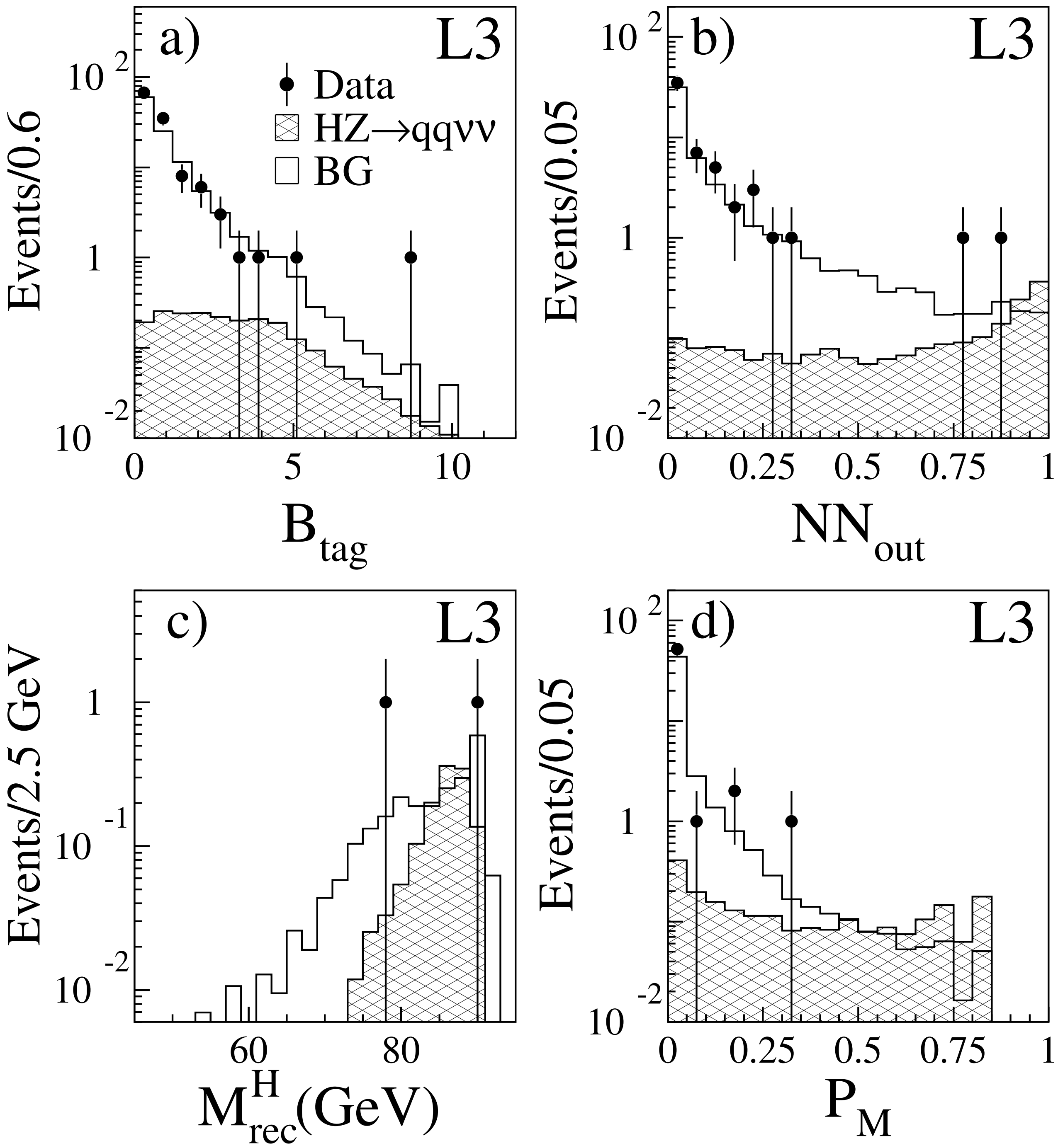

Figure 3: Distributions, shown after the preselection for the $q\bar{q}\nu\bar{\nu}$ channel, of (a) the event $B_{\rm tag}$ (before $B_{\rm tag} > 0.6$ cut), (b) the neural network output $NN_{\rm out}$, (c) the invariant mass (for events with $NN_{\rm out} > 0.5$) and (d) the purity. The dots indicate the data, the empty histograms show the background expectations, while the superimposed hatched histograms correspond to a 87 GeV Higgs signal normalised to the Standard Model cross section.

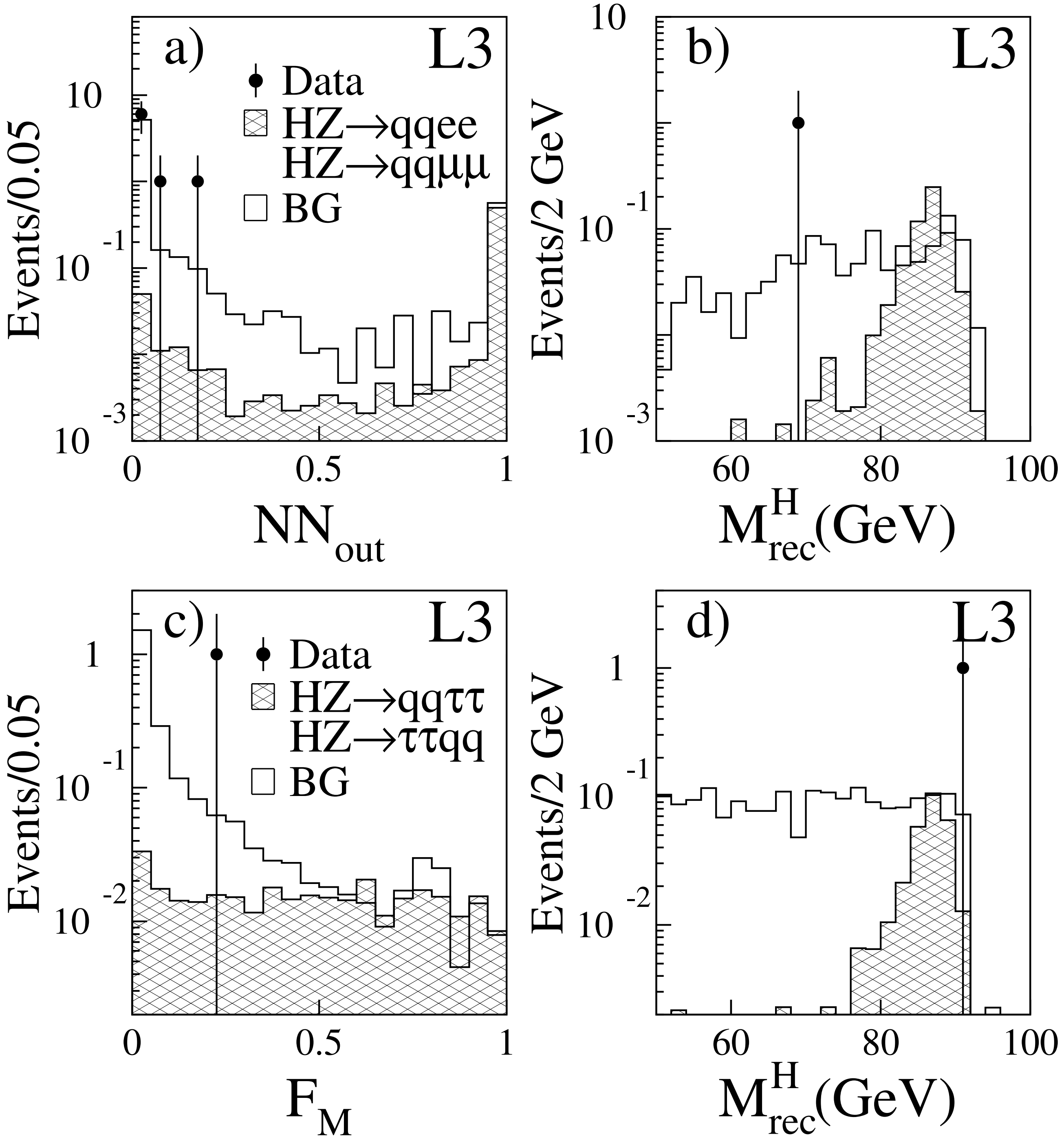

Figure 4: Distributions, after the preselection for the $q\bar{q}\,e^+e^-$ and $q\bar{q}\,\mu^+\mu^-$ channels combined, of (a) the neural network output $NN_{\rm out}$ and (b) the invariant mass (for events with $NN_{\rm out} > 0.1$); and distributions, after the final selections for the $q\bar{q}\,\tau^+\tau^-$ and $\tau^+\tau^-\,q\bar{q}$ channels combined, of (c) the mass probability F_M and (d) the reconstructed Higgs mass $M^{\rm H}_{\rm rec}$. The dots indicate the data, the empty histograms show the background expectations, while the superimposed hatched histograms correspond to a 87 GeV Higgs signal normalised to the Standard Model cross section.

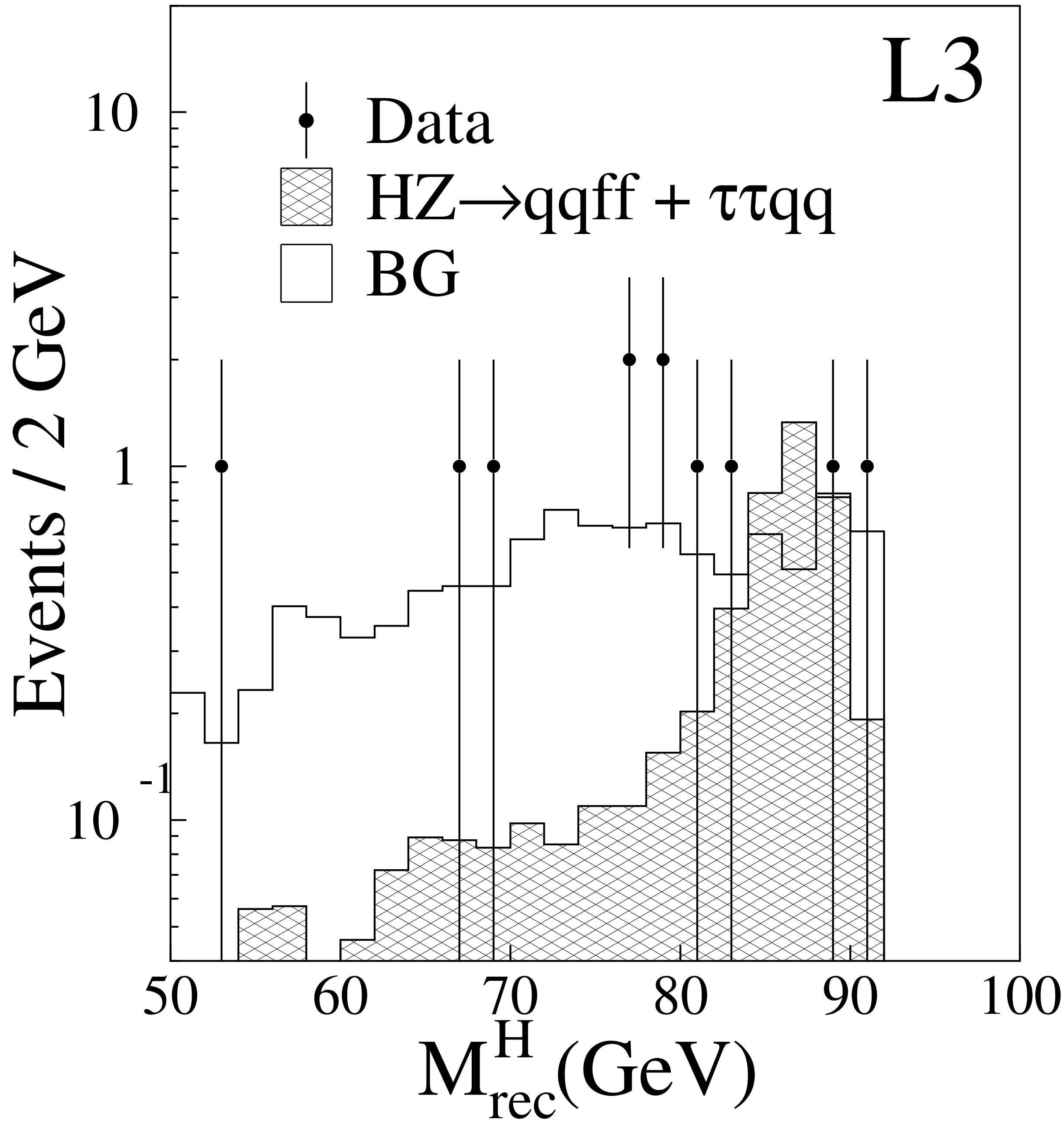

Figure 5: The reconstructed Higgs mass distribution of the 11 most significant candidates selected in the data with $NN_{\mathrm{out}} > 0.7$, 0.5 and 0.1 for the $\mathrm{q\bar{q}q\bar{q}}$, $\mathrm{q\bar{q}}\nu\bar{\nu}$ and $\mathrm{q\bar{q}}\ell^+\ell^-$ selections, respectively, and with $D_M > -3$ for the $\mathrm{q\bar{q}}\tau^+\tau^-$ and $\tau^+\tau^-\mathrm{q\bar{q}}$ selections. The corresponding distributions for an 87 GeV Higgs signal and for the background are also shown for comparison.

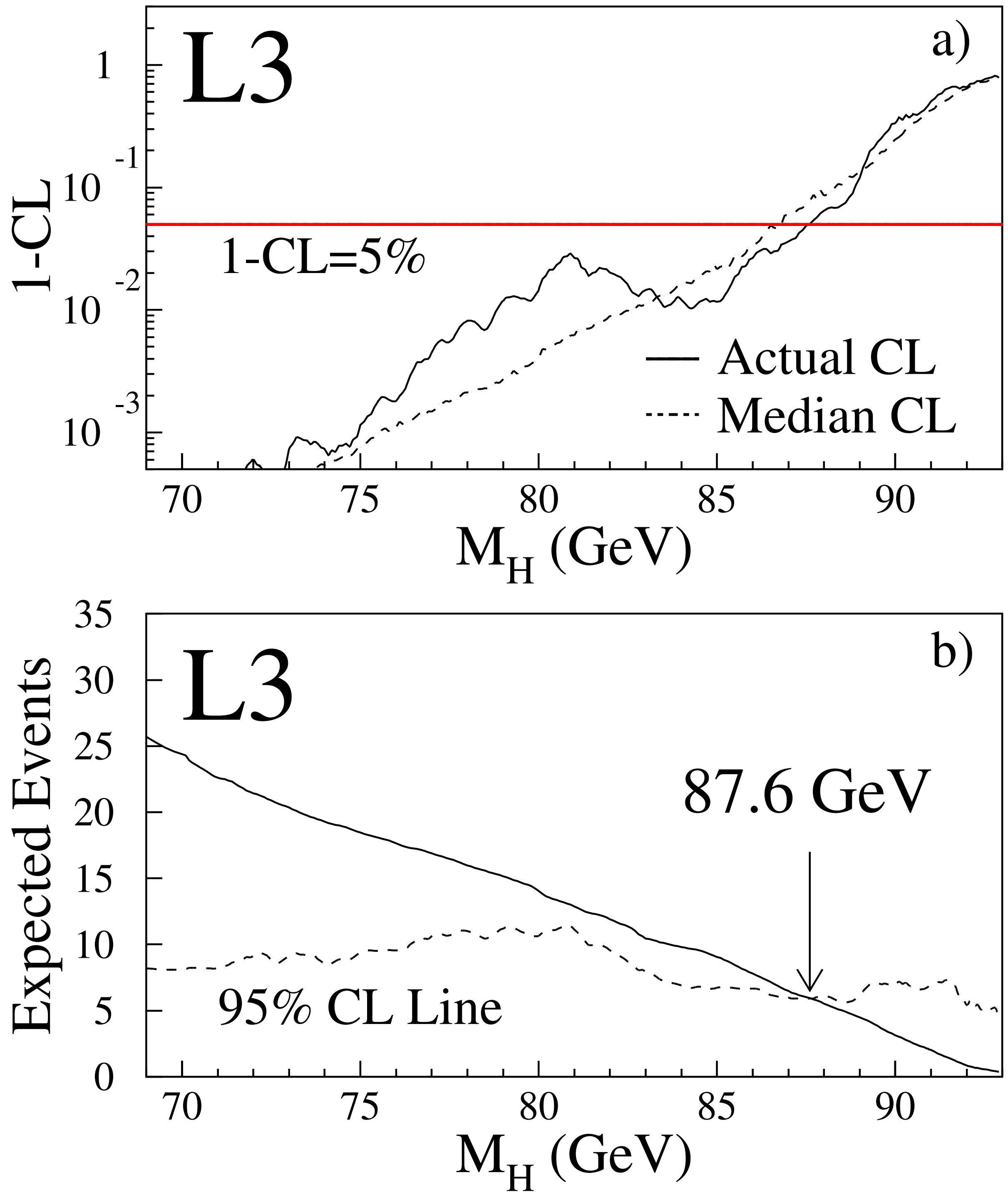

Figure 6: (a) The (1-CL) line for the Higgs signal derived from the data as a function of the Higgs mass (solid line). The median expectation, derived from the sample of Monte Carlo experiments, is indicated by the dotted line. (b) The number of expected signal events (solid line) together with the number of signal events excluded at 95% confidence level (dashed line).